

Band structure and electronic transport across Ta₂O₅/Nb:SrTiO₃ interfaces

Dror Miron,¹ Dana Cohen Azarzar,¹ Noa Segev,^{1,2} Maria Baskin,¹ Felix Palumbo,^{3,4} Eilam Yalon^{1,a)} and Lior Kornblum^{1,2,a)}

¹ *Andrew & Erna Viterbi Dept. of Electrical Engineering, Technion – Israel Institute of Technology, Haifa 32000-03, Israel*

² *The Grand Technion Energy Program (GTEP), Technion – Israel Institute of Technology, Haifa 32000-03, Israel*

³ *Unidad de Investigación y Desarrollo de las Ingenierías, Facultad Regional Buenos Aires, Universidad Tecnológica Nacional (UIDI FRBA-UTN), Medrano 951, C1179AAQ Buenos Aires, Argentina*

⁴ *Consejo Nacional de Investigaciones Científicas y Técnicas, Godoy Cruz 2290, C1425FQB Buenos Aires, Argentina*

Resistive switching devices promise significant progress in memory and logic technologies. One of the hurdles towards their practical realization is the high forming voltages required for their initial activation, which may be incompatible with standard microelectronics architectures. This work studies the conduction mechanisms of Ta₂O₅ layers, one of the most studied material for memristive devices, in their initial, as-fabricated state (“pre-forming”). By separating this aspect and resolving the current mechanisms, we provide input that may guide future design of resistive switching devices. For this purpose, Ta₂O₅ layers were sputtered on conductive Nb:SrTiO₃ substrates. Ta₂O₅/Nb:SrTiO₃ structures exhibit diode behavior with an ideality factor of $n \approx 1.3$ over 4 current decades. X-ray photoelectron spectroscopy analysis of the interfacial band offsets reveals a barrier of 1.3 ± 0.3 eV for electrons injected from the semiconductor into Ta₂O₅. Temperature-dependent current-voltage analysis exhibits rectifying behavior. While several conduction mechanisms produce good fits to the data, comparing the physical parameters of these models to the expected physical parameters led us to conclude that trap assisted tunneling (TAT) is the most likely conduction mechanism. Fitting the data using a recent TAT model and with the barrier that was measured by spectroscopy fully captures the temperature dependence, further validating this conduction mechanism.

^{a)} Authors to whom correspondence should be addressed. Eilam Yalon: eilamy@technion.ac.il, Lior Kornblum: liork@ee.technion.ac.il

I. Introduction

An interface between two dissimilar materials often governs the operation and performance of many important devices. In oxide electronics, devices are often based on phenomena offered by oxide interfaces, such as magnetism, ferroelectricity, superconductivity, 2D conductivity and others^{1,2}. Strontium titanate (SrTiO₃, STO) and its interfaces have gathered exceptional attention, which recently focused on their potential for novel devices²⁻⁴. Current injection through interfaces of STO with other materials has been the source of significant interest, in the context of devices such as magnetic tunnel junctions,⁵ photoelectrocatalytic hydrogen production,^{6,7} memristors^{8,9} and selector diodes^{10,11}. Tantalum oxide, or Ta₂O_{5- δ} (to be referred to as Ta₂O₅ for simplicity) is one of the most studied materials for resistive switching devices¹²⁻²⁰ and for diode selector for resistive random access memory array²¹.

Electroforming is a one-step process that must take place in resistive switching devices, which allows it to move from its initial highly resistive state to low resistive state. The forming voltages are usually much larger than the switching voltages and they are often incompatible²² with the operating voltages required in CMOS technology. Thus, it is desirable to optimize devices to lower forming voltages or to create a forming-free device²². Defects in Ta₂O₅, such as oxygen vacancies, play a major role in its electrical behavior,^{18,20,23,24} and they are one of the likely reasons for the reported dependence of the forming voltage on the stoichiometry of the layer¹⁹. Such defects also have a profound effect on the conduction mechanism²⁵. Therefore, understanding the conduction mechanism may shed light on the defect properties and their electrical manifestation. In this light, several conduction mechanisms have been considered for this system, including

Poole-Frenkel emission and hopping between defects on the one hand,²⁶ and defect-less mechanisms such as thermionic emission and tunneling between electrodes on the other²¹.

We address this problem by studying the conduction mechanisms in Ta₂O₅/STO structures. We employ Nb-doped STO as the substrate owing to its advantage as a back electrode: unlike semiconductor substrates (e.g. Si), no insulating interfacial layer²⁷ is expected here, simplifying the analysis.²⁵ In addition, this oxide-oxide interface can be analyzed by spectroscopy to produce a picture of the energy barriers, which play an important role in the assessment of charge transport mechanisms.

In this work the electronic structure of Ta₂O₅/STO interfaces is measured by spectroscopy, and then correlated with temperature-dependent electronic transport. This work does not address memristive effects, which are intentionally negligible in the present configuration of the samples, mostly due to their high oxygen content.¹⁹ Nonetheless, this configuration mimics the pre-forming state in Ta₂O₅ based memristors, where STO is useful as a well-understood back electrode. Accordingly, these results may promote the understanding of memristor devices in their pre-forming regime, provide guidelines for optimizing their design and the design of other devices such as oxide diodes and selectors.^{10,11}

II. Experimental

Doped (001) STO substrates (0.01% wt. Nb, CrysTec GmbH) were TiO₂-terminated using the 'extended Arkansas' method.²⁸ Amorphous Ta₂O₅ layers were reactively sputtered (AJA International ATC 2200) at room temperature using a Ta₂O₅ target. A flow of 10:50 sccm O₂:Ar was used at a pressure of 3 mTorr and power of 180 W. Oxygen-rich conditions were chosen to

reduce the defects and associated memristive behavior,¹⁹ in order to provide a simple test case for the transport analysis. Then 50 nm thick circular Pt top contacts and a 300 nm thick Al blanket back contact were deposited using e-beam evaporation, with the Pt pads (measured area of $6 \cdot 10^{-4}$ cm² using light microscope) deposited through a shadow mask. X-ray photoelectron spectroscopy (XPS, Physical Electronics VersaProbe III) was performed with monochromated Al K α source and a pass energy of 11.75 eV, and analyzed using CasaXPS with a Shirley background. The energy scale is aligned such as that C 1s peaks are at 285 eV, although no absolute energies are used throughout the analysis. Current-density voltage (JV) measurements were conducted using Keithely 2450 source meter instrument, in a shielded box with a home-built heating stage.

III. Results

The spectroscopic analysis of the band offsets at the interface is based on comparison of ‘thin’ and ‘thick’ Ta₂O₅ layers and a bare Nb:STO substrate.^{29–32} ‘Thin’ refers to a layer thin enough for XPS to be able to acquire information from both the Ta₂O₅ layer and the underlying substrate, and 3.1 and 9.9 nm layers were deposited for the thin and thick samples (± 0.5 nm, measured by ellipsometry), respectively. The Ta 4f spectra of the thin and thick samples were fitted with a single f-doublet, indicative of predominantly Ta⁺⁵ (Ta₂O₅) species; the Ti 2p spectrum of the thin sample (acquired from underneath Ta₂O₅) exhibits a small +3 component in addition to the major +4 state. A Ta₂O₅ band gap value of 4.8 ± 0.3 eV is determined from the electron energy loss tail near the O 1s of the thick sample, where only Ta₂O₅ is probed. The details of this procedure were reported elsewhere for atomic layer deposited (ALD) Ta₂O₅ films,³³ where a value of $E_g = 4.5 \pm 0.2$ eV has been reported, in agreement to the current work and to other reports^{34,35}.

To obtain the Ta₂O₅-STO band offsets, we account for the Ti 2p, Ta 4f and valence band edge (VBE) spectral regions (Fig. 1a). For the thick (bare) sample, the distance between the Ta 4f

(Ti 2p) core level and the VBE has been measured, $\Delta E_{\text{Ta4f-VBE}}$ ($\Delta E_{\text{Ti2p-VBE}}$). It is emphasized that only energetic distances are used here and the absolute peak positions, although calibrated, are unnecessary for the analysis. For the thin sample, the energy distance between the Ta 4f and Ti 2p core levels ($\Delta E_{\text{Ti2p-Ta4f}}$) has been measured. By rearrangement of these differences^{31,36,37} a relative valence band offset, VBO, of $\Delta E_{\text{Ti2p-VBE}} - \Delta E_{\text{Ti2p-Ta4f}} - \Delta E_{\text{Ta4f-VBE}} = 0.3 \pm 0.15$ eV is determined. Taking the band gap of STO as 3.2 eV and that of Ta₂O₅ as 4.8 eV, a conduction band offset (CBO) of 1.3 ± 0.3 eV is calculated across the interface (Fig. 1b).

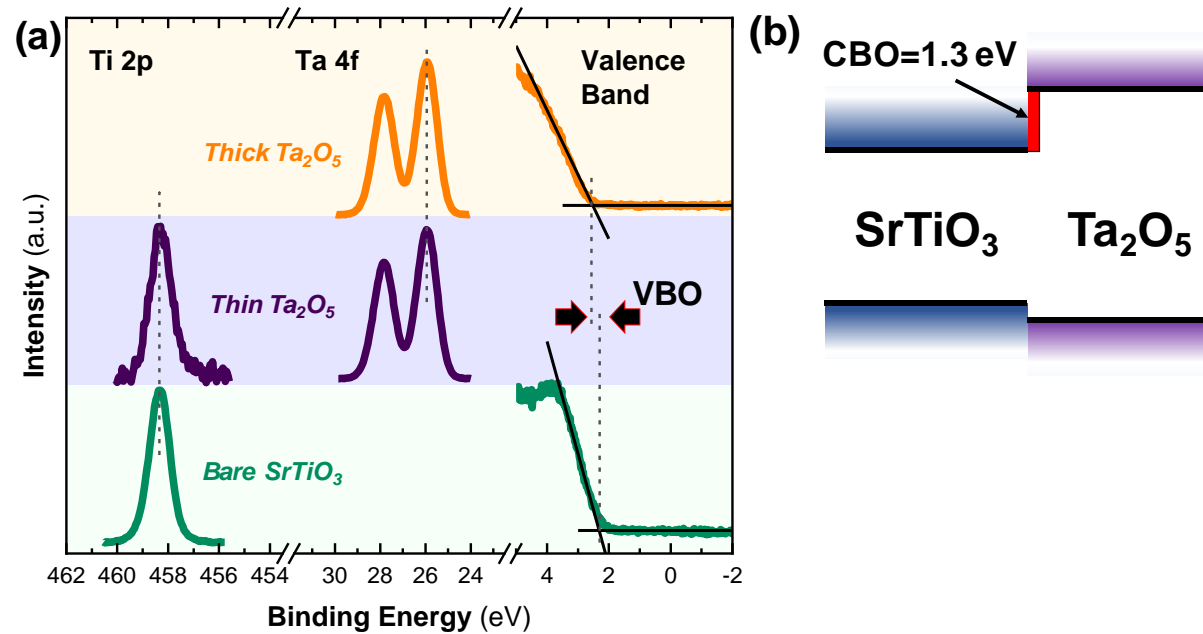


Figure 1. XPS analysis of the band offsets at Ta₂O₅/Nb:STO interface. (a) Comparison of the core levels Ta 4f and Ti 2p and the valence band spectra of thick and thin Ta₂O₅ layers on Nb:STO, and those of a bare substrate. The measured valence band offset is denoted by thick arrows. Core level spectra are shown after background subtraction. (b) The resulting band diagram, with the conduction band offset (CBO) denoted by a red bar.

Further analysis of the interfacial electronic properties is performed by current-voltage measurements. JV measurements (Fig. 2b) exhibit a diode-like behavior with currents below the

measurement noise at voltages below 0.5 V (positive voltage is defined as positive voltage on the Pt pad). High current rise rate of 78 mV/decade is determined (Fig. 2b inset), which is in proximity to the value of 60 mV/decade of an ideal diode, producing an ideality factor of $n \approx 1.3$. We focus on the positive voltage region (defined as positive voltage on the top Pt pad) in order to understand the conduction mechanisms and determine how and whether they are related to the barrier defined by the Ta₂O₅-STO band offsets (Fig. 1b), whereas the negative voltage behavior is expected to be governed by the large Pt-Ta₂O₅ barrier. However, no negative voltage currents were observed above the noise floor, which we ascribe to a possible depletion region in the low-doped STO, upon which most of the voltage drops. This has no consequence on the positive voltage analysis, where no depletion layer exists. We note that if the current blocking at negative voltage is indeed caused by an STO depletion layer, similar current blocking is expected even for the less insulating sub-stoichiometric Ta oxides, that are typically used in memristors.

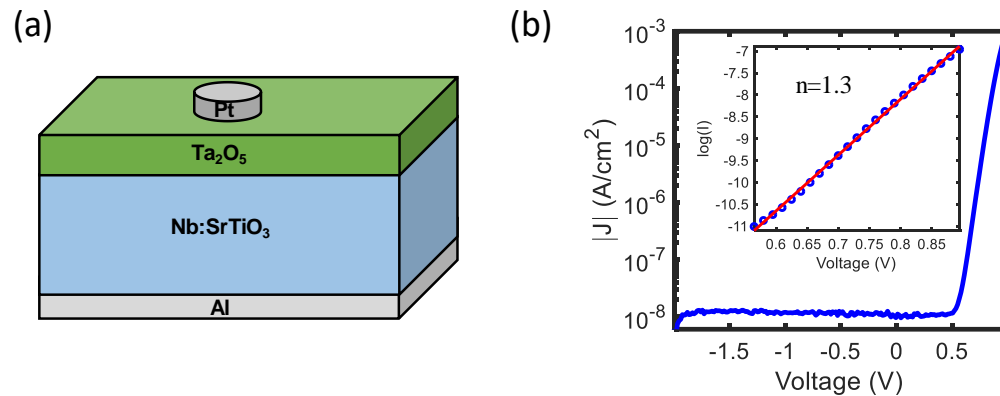


Figure 2. (a) Schematic view of the device structure and (b) room temperature current-density characteristics of Pt/Ta₂O₅/STO structures. Inset: linear fitting of the logarithm of the current in the range 0.55-0.9 V, resulting in a current rise rate of 78 mV/decade. Positive voltage on the Pt gate pad is defined as positive voltage.

To address the question of the dominant conduction mechanism in positive voltage, four different mechanisms have been considered: Poole-Frenkel (PF) emission, Schottky-Richardson thermionic emission (TE), trap-assisted tunneling (TAT) and Fowler-Nordheim tunneling³⁸ (FNT). JV measurements were conducted at temperatures of 22-80 °C (Fig. 3a). A distinct increase of the current density is observed with temperature, implying that the conduction mechanism is temperature-dependent. This observation precludes FNT, which in its most simplified form is temperature-independent. While both PF and TE conduction mechanisms enable decent fits, these fits yield permittivity values that are far from anything that can be physically reasonable. As was recently shown, the extracted parameters of such analyses are strongly dependent of the assumed flat-band voltage (V_{FB}), which is necessary for relating between the applied voltage and the field on the insulator. Following our recent discussion,²⁵ a wide flat-band voltage range of ± 3 V did not yield physically plausible values for the permittivity (Fig. S1). This therefore excludes PF and TE as reasonable conduction mechanisms here.

Trap assisted tunneling (TAT) is a general name that encapsulates many different models with a wide range of assumptions and variants³⁹⁻⁴². A general approach to describe TAT is by a two-step process, where the electron first tunnels from the injecting cathode (STO here) to a trap state in the insulator (Ta_2O_5), followed by tunneling of the electron to the anode (Pt here). We first consider the simplified TAT model proposed by Fleischer et al., that describes the current density as follows⁴³:

$$J = 2C_t N_t q \phi_t \cdot (3E)^{-1} \exp(-A\phi_t^{-3/2} E^{-1}) \quad (1)$$

where C_t is a slowly varying function of electron energy, N_t the trap density, q is the elementary charge, ϕ_t the trap level versus the Ta_2O_5 conduction band, $A = 4\sqrt{2qm^*} \cdot (3\hbar)^{-1}$, $m^*=0.5m_0$ (Ref ⁴⁴) is the electron effective mass in Ta_2O_5 and \hbar is the reduced Planck constant.

The behavior of $\ln(JE)$ as a function of E^{-1} is linear (Fig. S2), supporting the validity of TAT and Eq. (1). Despite the agreement to the data, this model does not capture the temperature dependence and it assumes a temperature independent tunneling process. Therefore, while Fleischer's model provides an indication of TAT, it does not explain the behavior observed in Fig. 3a. More recently Yu et al. proposed a temperature-dependent TAT picture,⁴⁵ where the Fermi-Dirac distribution is used to describe the electron distribution in the injecting cathode (STO) (Fig. 3b). To apply this model to the data, we used the barrier height of 1.3 eV as obtained from XPS (Fig. 1b), an effective electron mass in the Ta₂O₅ layer of 0.5m₀ (Ref⁴⁴), and fitted the trap energy (ϕ_t) of 0.52 V below the conduction band of Ta₂O₅ and a density of 10²⁰ traps/cm³ (see Table S1 for the complete parameter set). While the electric field across the Ta₂O₅ layer is dependent on unknown parameters such as the band bending in the STO and the flat band voltage⁴⁶, in this simulation it is used as a fitting parameter and hence these parameters are irrelevant by themselves. We note that the field is assumed to be uniform across the Ta₂O₅ layer. Regarding the trap energy, theoretical and experimental works on several Ta oxide phases reported O vacancy energy levels of 0.6-1.5 eV below the conduction band,⁴⁷⁻⁵⁰ in decent agreement with the above. These parameters produce an accurate fit to the data (Fig. 3a), which captures both the XPS measured barriers and the temperature dependence. This agreement provides strong indication of TAT and Yu's model as the dominant conduction mechanism in the structures studied here. The Tsu-Esaki model was also considered to explain similar temperature dependent tunneling without an assumption of high density traps inside the dielectric⁵¹⁻⁵³. However, when the dielectric is thick enough, current flow near the Fermi level of the insulator dominates the conduction⁵⁴, and thus no temperature dependence is expected.

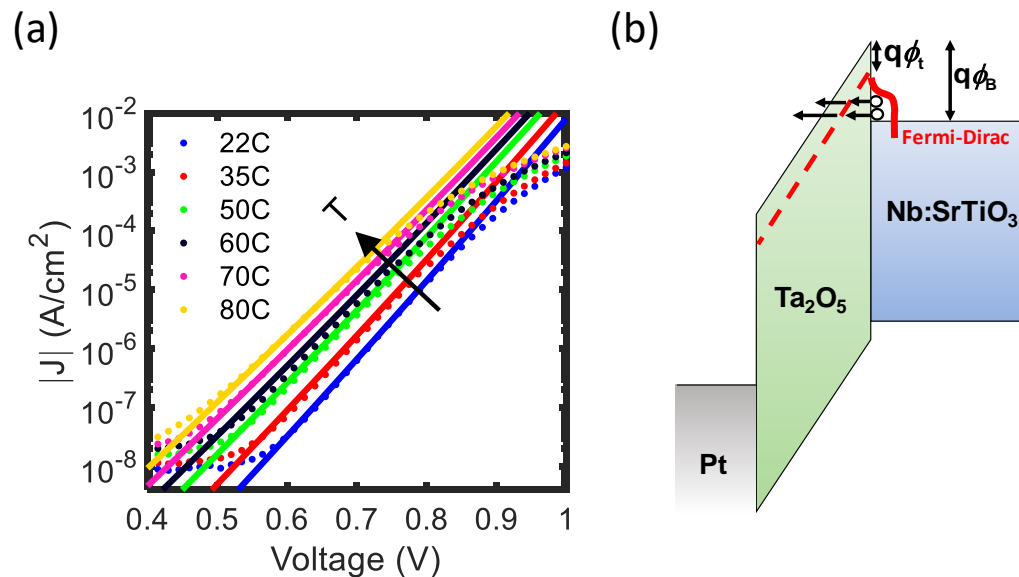


Figure 3. (a) JV measurements and TAT simulation using the model proposed by Yu et. al⁴⁵ at temperatures of 25-80 °C, with $\phi_t = 0.52$ V and $N_t = 10^{20}$ traps/cm³ as fitting parameters and (b) schematic view of this TAT conduction mechanism. The Fermi level position in the degenerately-doped Nb:STO is near the conduction band minimum.

We note that the sample showed some variability between different pads, which is ascribed to spatial non-uniformity of the traps in the Ta₂O₅ layer.⁵⁵ Nonetheless, for each one of the different pads, Yu's TAT model successfully captures their behavior, with some variations in trap parameters, consistent with Ta₂O₅ non-uniformity.

The deviation of the currents from the simulated TAT model at $V \gtrsim 0.9$ V may appear to be the effect of large series resistance, which may result from contacts and instrumentation. To assess this possibility one of the pads was electrically broken-down, to produce a near-Ohmic behavior (Fig. S3), resulting in ~ 4 k Ω which we estimate to be a conservative upper bound for the series resistor. However, even a 10 k Ω resistor is expected to produce a negligible deviation of 0.01 V in the voltage drop on the stack, since the current measured at 1 V is above 0.7 μ A. Therefore, series resistance is insufficient to explain this behavior. Alternatively, the active Ta₂O₅

traps may be filled at high current densities, causing a transition of the conduction mechanism to one that is based on electrons de-trapping by tunneling to the Pt electrode, which is assumed to be much less temperature dependent. Further analysis is required for a less speculative description of this effect.

The identification of the conduction mechanism of as-deposited Ta₂O₅ as TAT based on oxygen deficiency, may help strengthen the understanding of the forming voltage dependence on the stoichiometry that was published on Ta₂O₅-based memristors. For example, Skaja et al. have shown that their pre-forming Ta₂O₅ memristors have ~30% higher forming voltage and more than ×2 higher initial pre-forming resistance for near-stoichiometric films, versus oxygen-deficient ones.¹⁹ Wang et al. have studied similar structures with more complex oxygen profiles, and similarly observed lower initial resistance in the oxygen-deficient films¹⁷ (albeit with higher forming voltages). From the conduction mechanisms perspective, these observations can be explained by higher concentration of oxygen vacancy traps in the oxygen-deficient films, that play a role in the forming process.

IV. Conclusions

This work addressed the electronic properties of Ta₂O₅ layers sputtered on STO crystals with high oxygen content. These structures exhibit rectifying diode behavior. XPS analysis revealed a conduction band offset of 1.3 eV, functioning as a barrier for electrons emitted from STO to Ta₂O₅. The positive voltage currents are modeled by TAT mechanism. Using the TAT model proposed by Yu et al.⁴⁵ we were able to capture the physical parameters of the conduction, using the barrier acquired by XPS and including the temperature dependence. The results are discussed within the context of pre-forming Ta₂O₅ memristor, and comparison to published data suggest that our observations apply to other works. We note that with devices featuring lower

barriers than that reported here for Ta₂O₅/STO, thermionic emission is expected to play a more important role.^{52,53}

V. Supplemental Material

Evaluation of TE and PF as conduction mechanisms, details of Fleischer's TAT model, derivation of Yu's model and its parameters, and discussion of the absence of a significant series resistance can be found in the Supplemental Material.

Data Availability

The entire raw data used to plot the figures of this work is available in an annotated xlsx file, available in the Supplemental Materials

Acknowledgements

This work was funded by a Nevet (Seed) Project from the Grand Technion Energy Program (GTEP) and by the Israeli Ministry of Energy (MoE). Sample fabrication and characterization was done with the support of the Technion's Micro-Nano Fabrication and Printing Unit (MNF&PU) and the Russell Berrie Nanotechnology Institute (RBNI). The authors thank Dr. Guy Ankonina from the Technion for his expertise and assistance with sputtering of the layers, and Dr. Larisa Burstein from Tel-Aviv University for her expertise with XPS. LK is a Chanin Fellow.

References

- ¹ H.Y. Hwang, Y. Iwasa, M. Kawasaki, B. Keimer, N. Nagaosa, and Y. Tokura, *Nat Mater* **11**, 103 (2012).
- ² L. Kornblum, *Adv. Mater. Interfaces* **6**, 1900480 (2019).
- ³ Z. Liu, A. Annadi, and Ariando, in *Funct. Mater. Electron.* (Apple Academic Press, New York, 2018), pp. 35–95.
- ⁴ N. Pryds and V. Esposito, *J. Electroceramics* **38**, 1 (2016).
- ⁵ A.M. Kamerbeek, R. Ruiter, and T. Banerjee, *Sci. Rep.* **8**, 1378 (2018).
- ⁶ L. Ji, M.D. McDaniel, S. Wang, A.B. Posadas, X. Li, H. Huang, J.C. Lee, A.A. Demkov, A.J. Bard, J.G. Ekerdt, and E.T. Yu, *Nat Nano* **10**, 84 (2015).
- ⁷ L. Kornblum, D.P. Fenning, J. Faucher, J. Hwang, A. Boni, M.G. Han, M.D. Morales-Acosta, Y. Zhu,

This is the author's peer reviewed, accepted manuscript. However, the online version of record will be different from this version once it has been copyedited and typeset.
PLEASE CITE THIS ARTICLE AS DOI: 10.1063/1.5139533

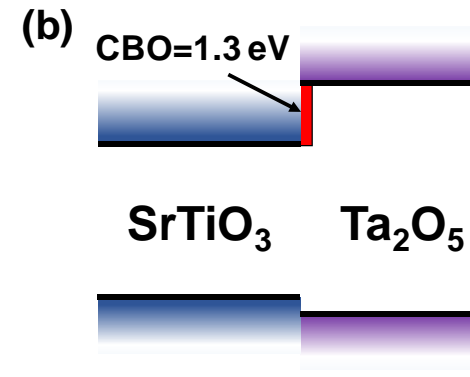
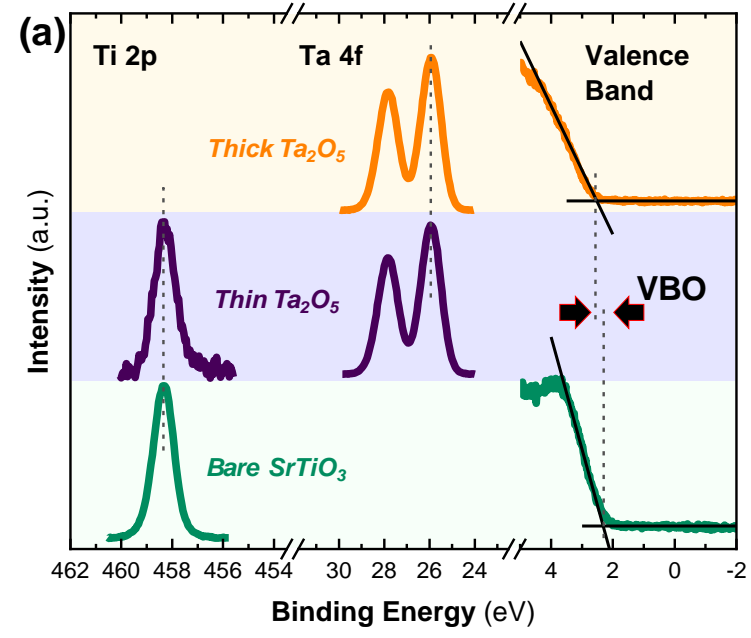
- E.I. Altman, M.L. Lee, C.H. Ahn, F.J. Walker, and Y. Shao-Horn, *Energy Environ. Sci.* **10**, 377 (2017).
- ⁸ A.S. Goossens, A. Das, and T. Banerjee, *J. Appl. Phys.* **124**, 152102 (2018).
- ⁹ R. Dittmann, R. Muenstermann, I. Krug, D. Park, T. Menke, J. Mayer, A. Besmehn, F. Kronast, C.M. Schneider, and R. Waser, *Proc. IEEE* **100**, 1979 (2012).
- ¹⁰ T. Moon, H.J. Jung, Y.J. Kim, M.H. Park, H.J. Kim, K. Do Kim, Y.H. Lee, S.D. Hyun, H.W. Park, S.W. Lee, and C.S. Hwang, *APL Mater.* **5**, 42301 (2016).
- ¹¹ T. Moon, H.J. Lee, K. Do Kim, Y.H. Lee, S.D. Hyun, H.W. Park, Y. Bin Lee, B.S. Kim, and C.S. Hwang, *Adv. Electron. Mater.* **4**, 1800388 (2018).
- ¹² K.M. Kim, S.R. Lee, S. Kim, M. Chang, and C.S. Hwang, *Adv. Funct. Mater.* **25**, 1527 (2015).
- ¹³ T.H. Park, S.J. Song, H.J. Kim, S.G. Kim, S. Chung, B.Y. Kim, K.J. Lee, K.M. Kim, B.J. Choi, and C.S. Hwang, *Sci. Rep.* **5**, 15965 (2015).
- ¹⁴ G.-S. Park, Y.B. Kim, S.Y. Park, X.S. Li, S. Heo, M.-J. Lee, M. Chang, J.H. Kwon, M. Kim, U.-I. Chung, R. Dittmann, R. Waser, and K. Kim, *Nat. Commun.* **4**, 2382 (2013).
- ¹⁵ T. Breuer, A. Siemon, E. Linn, S. Menzel, R. Waser, and V. Rana, *Nanotechnology* **26**, 415202 (2015).
- ¹⁶ T. Breuer, L. Nielen, B. Roesgen, R. Waser, V. Rana, and E. Linn, *Sci. Rep.* **6**, 23967 (2016).
- ¹⁷ B. Wang, K.H. Xue, H.J. Sun, Z.N. Li, W. Wu, P. Yan, N. Liu, B.Y. Tian, X.X. Liu, and X.S. Miao, *Appl. Phys. Lett.* **113**, 183501 (2018).
- ¹⁸ C.M.M. Rosário, B. Thöner, A. Schönhals, S. Menzel, A. Meledin, N.P. Barradas, E. Alves, J. Mayer, M. Wuttig, R. Waser, N.A. Sobolev, and D.J. Wouters, *Nanoscale* (2019).
- ¹⁹ K. Skaja, M. Andrä, V. Rana, R. Waser, R. Dittmann, and C. Baeumer, *Sci. Rep.* **8**, 10861 (2018).
- ²⁰ S. Kim, S. Choi, and W. Lu, *ACS Nano* **8**, 2369 (2014).
- ²¹ M. Wang, J. Zhou, Y. Yang, S. Gaba, M. Liu, and W.D. Lu, *Nanoscale* **7**, 4964 (2015).
- ²² W. Kim, D.J. Wouters, S. Menzel, C. Rodenbücher, R. Waser, and V. Rana, in *2016 46th Eur. Solid-State Device Res. Conf.* (2016), pp. 164–167.
- ²³ A. Tsurumaki-Fukuchi, R. Nakagawa, M. Arita, and Y. Takahashi, *ACS Appl. Mater. Interfaces* **10**, 5609 (2018).
- ²⁴ W. Kim, A. Hardtdegen, C. Rodenbücher, S. Menzel, D.J. Wouters, S. Hoffmann-Eifert, D. Buca, R. Waser, and V. Rana, in *2016 IEEE Int. Electron Devices Meet.* (2016), pp. 4.4.1-4.4.4.
- ²⁵ D. Miron, I. Krylov, M. Baskin, E. Yalon, and L. Kornblum, *J. Appl. Phys.* **126**, 185301 (2019).
- ²⁶ A.A. Sharma, M. Noman, M. Abdelmoula, M. Skowronski, and J.A. Bain, *Adv. Funct. Mater.* **24**, 5522 (2014).
- ²⁷ W.J. Maeng, S.-J. Park, and H. Kim, *J. Vac. Sci. Technol. B Microelectron. Nanom. Struct. Process. Meas. Phenom.* **24**, 2276 (2006).
- ²⁸ J. Zhang, D. Douth, T. Merz, J. Chakhalian, M. Kareev, J. Liu, and L.J. Brillson, *Appl. Phys. Lett.* **94**, 092904 (2009).
- ²⁹ S.A. Chambers, Y. Du, R.B. Comes, S.R. Spurgeon, and P. V Sushko, *Appl. Phys. Lett.* **110**, 82104 (2017).
- ³⁰ Z.H. Lim, K. Ahmadi-Majlan, E.D. Grimley, Y. Du, M. Bowden, R. Moghadam, J.M. LeBeau, S.A. Chambers, and J.H. Ngai, *J. Appl. Phys.* **122**, 84102 (2017).
- ³¹ L. Kornblum, M.D. Morales-Acosta, E.N. Jin, C.H. Ahn, and F.J. Walker, *Adv. Mater. Interfaces* **2**, 201500193 (2015).
- ³² D. Cohen-Azarzar, M. Baskin, and L. Kornblum, *J. Appl. Phys.* **123**, 245307 (2018).
- ³³ L. Kornblum, B. Meyler, J. Salzman, and M. Eizenberg, *J. Appl. Phys.* **113**, 074102 (2013).
- ³⁴ S. Miyazaki, *Appl. Surf. Sci.* **190**, 66 (2002).
- ³⁵ J. Robertson and R.M. Wallace, *Mater. Sci. Eng. R Reports* **88**, 1 (2015).
- ³⁶ S.A. Chambers, Y. Liang, Z. Yu, R. Droopad, J. Ramdani, and K. Eisenbeiser, *Appl. Phys. Lett.* **77**, 1662 (2000).
- ³⁷ K.J. May, D.P. Fenning, T. Ming, W.T. Hong, D. Lee, K.A. Stoerzinger, M.D. Biegalski, A.M. Kolpak, and Y. Shao-Horn, *J. Phys. Chem. Lett.* **6**, 977 (2015).
- ³⁸ S.M. Sze and K.K. Ng, *The Physics of Semiconductor Devices*, 3rd ed. (Wiley, 2007).
- ³⁹ C. Svensson and I. Lundström, *J. Appl. Phys.* **44**, 4657 (1973).

This is the author's peer reviewed, accepted manuscript. However, the online version of record will be different from this version once it has been copyedited and typeset.

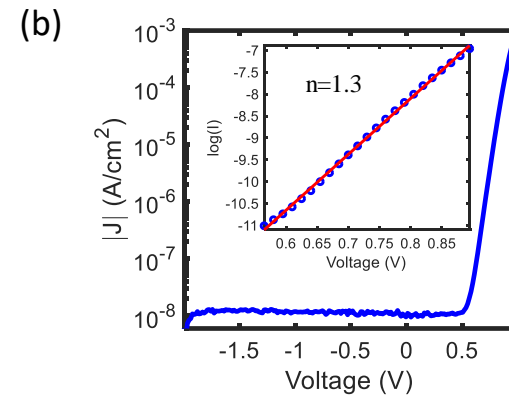
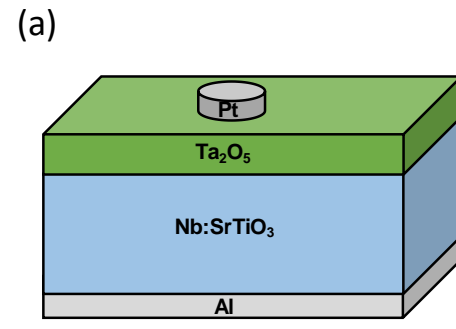
PLEASE CITE THIS ARTICLE AS DOI: 10.1063/1.5139533

- ⁴⁰ M.P. Houngh, Y.H. Wang, and W.J. Chang, *J. Appl. Phys.* **86**, 1488 (1999).
- ⁴¹ M. Houssa, M. Tuominen, M. Naili, V. Afanas'ev, A. Stesmans, S. Haukka, and M.M. Heyns, *J. Appl. Phys.* **87**, 8615 (2000).
- ⁴² M.A. Bhuiyan, H. Zhou, R. Jiang, E.X. Zhang, D.M. Fleetwood, P.D. Ye, and T.-P. Ma, *IEEE Electron Device Lett.* **39**, 1022 (2018).
- ⁴³ S. Fleischer, P.T. Lai, and Y.C. Cheng, *J. Appl. Phys.* **73**, 3348 (1993).
- ⁴⁴ B.C.M. Lai, N.H. Kung, J.Y.M. Lee, and others, *J. Appl. Phys.* **85**, 4087 (1999).
- ⁴⁵ S. Yu, X. Guan, and H.-S.P. Wong, *Appl. Phys. Lett.* **99**, 63507 (2011).
- ⁴⁶ Y. Taur and T.H. Ning, *Fundamentals of Modern VLSI Devices* (Cambridge university press, 2013).
- ⁴⁷ V. Mikhaelashvili, Y. Betzer, I. Prudnikov, M. Orenstein, D. Ritter, and G. Eisenstein, *J. Appl. Phys.* **84**, 6747 (1998).
- ⁴⁸ B. Xiao and S. Watanabe, *Nanoscale* **6**, 10169 (2014).
- ⁴⁹ Y. Guo and J. Robertson, *Microelectron. Eng.* **147**, 254 (2015).
- ⁵⁰ J. Lee, W.D. Lu, and E. Kioupakis, *Nanoscale* **9**, 1120 (2017).
- ⁵¹ R. Tsu and L. Esaki, *Appl. Phys. Lett.* **22**, 562 (1973).
- ⁵² C. Funck, A. Marchewka, C. Bäumer, P.C. Schmidt, P. Müller, R. Dittmann, M. Martin, R. Waser, and S. Menzel, *Adv. Electron. Mater.* **4**, 1800062 (n.d.).
- ⁵³ C. Baeumer, C. Funck, A. Locatelli, T.O. Menteş, F. Genuzio, T. Heisig, F. Hensling, N. Raab, C.M. Schneider, S. Menzel, R. Waser, and R. Dittmann, *Nano Lett.* **19**, 54 (2019).
- ⁵⁴ E. Yalon, I. Riess, and D. Ritter, *IEEE Trans. Electron Devices* **61**, 1137 (2014).
- ⁵⁵ Q. Xu, Y. Ma, and M. Skowronski, *J. Appl. Phys.* **127**, 55107 (2020).

This is the author's peer reviewed, accepted manuscript. However, the online version of record will be different from this version once it has been copyedited and typeset.
PLEASE CITE THIS ARTICLE AS DOI: 10.1063/1.5139533



This is the author's peer reviewed, accepted manuscript. However, the online version of record will be different from this version once it has been copyedited and typeset.
PLEASE CITE THIS ARTICLE AS DOI: 10.1063/1.5139533



This is the author's peer reviewed, accepted manuscript. However, the online version of record will be different from this version once it has been copyedited and typeset.
PLEASE CITE THIS ARTICLE AS DOI: 10.1063/1.5139533

